

## Article

# Experimental Study on the Performance of Glass/Basalt Fiber Reinforced Concrete Unidirectional Plate under Impact Load

Liancheng Li <sup>1</sup>, Jueliang Chen <sup>2</sup>, Siyu Liu <sup>2,\*</sup>, Xin Huang <sup>3</sup> and Hui Chen <sup>2,\*</sup>

<sup>1</sup> College of Architecture and Civil Engineering, Wenzhou University, Wenzhou 325035, China; 21461544036@stu.wzu.edu.cn

<sup>2</sup> Wenzhou Key Laboratory of Intelligent Lifeline Protection and Emergency Technology for Resilient City, College of Architecture and Energy Engineering, Wenzhou University of Technology, Wenzhou 325035, China; jueliang\_chen@yahoo.com

<sup>3</sup> Wenzhou Traffic Engineering Testing and Testing Co., Ltd., Wenzhou 325035, China; 20461542031@stu.wzu.edu.cn

\* Correspondence: liyalisiyu@yahoo.com (S.L.); chenhui0306@wzu.edu.cn (H.C.)

**Abstract:** Fiber-reinforced composite materials have emerged as essential solutions for addressing the durability challenges of traditional reinforced concrete, owing to their lightweight nature, high strength, ease of construction, superior tensile capacity, robust corrosion resistance, and excellent electromagnetic insulation properties. This paper delves into the influence of loading rate and fiber bar type on the mechanical characteristics of concrete one-way plates through impact experiments on such plates fitted with glass/basalt fiber bars at varying drop weight heights. The test results reveal a direct correlation between increasing loading rates and escalating damage in fiber-reinforced concrete one-way plates, reflected in the progressive rise in peak deflection and residual displacement at the mid-span of the specimens. Notably, when subjected to higher impact loads, glass fiber-reinforced concrete specimens exhibit amplified deformation and intricate crack formations, consequently diminishing the overall deformation resistance of the plate. Furthermore, glass/basalt fiber-reinforced composites demonstrate notable vibration damping qualities, characterized by substantial residual displacement, minimal rebound, and rapid decay following vibration stimulation. Overall, glass fiber-reinforced one-way plates display marginally superior impact resistance compared to their basalt fiber-reinforced counterparts.

**Keywords:** glass/basalt fiber bar; impact load; loading rate; mid-span deflection; mechanical properties



**Citation:** Li, L.; Chen, J.; Liu, S.; Huang, X.; Chen, H. Experimental Study on the Performance of Glass/Basalt Fiber Reinforced Concrete Unidirectional Plate under Impact Load. *Buildings* **2024**, *14*, 1367. <https://doi.org/10.3390/buildings14051367>

Academic Editor: Fabio Di Trapani

Received: 31 March 2024

Revised: 28 April 2024

Accepted: 7 May 2024

Published: 10 May 2024



**Copyright:** © 2024 by the authors. Licensee MDPI, Basel, Switzerland. This article is an open access article distributed under the terms and conditions of the Creative Commons Attribution (CC BY) license (<https://creativecommons.org/licenses/by/4.0/>).

## 1. Introduction

Fiber-reinforced polymer (FRP) bars have garnered significant attention due to their high strength, light weight, and excellent fatigue resistance. They exhibit substantial potential in replacing steel bars in concrete structures, thereby enhancing the durability and performance of concrete structures [1]. Glass fiber-reinforced polymer (GFRP), in particular, possesses a thermal expansion coefficient similar to that of concrete, enabling cooperative deformation with changes in external temperature and hence reducing temperature-induced stress [2,3]. Nonetheless, the elastic modulus of FRP typically ranges from 25% to 70% of that of conventional steel bars [4–6], resulting in pronounced deflection and wide cracks in FRP concrete structures under stress [7,8].

Moreover, composite materials demonstrate outstanding vibration damping properties and high natural frequencies, effectively mitigating early resonance occurrences. These materials also exhibit significant internal damping, facilitating rapid attenuation of vibrations [9,10]. Studies on the bond strength between basalt fiber bars and concrete indicate a range from 11.592 to 23.578 MPa, with this strength being influenced by variations in thread depth and spacing [11,12]. Additionally, the strength and elastic modulus of glass

fiber bars diminish with increasing temperature, particularly with a sharp strength decline beyond 270 °C [13,14].

Previous studies have indicated that marine environments with chlorine salt corrosion pose a significant risk to traditional steel bars, leading to rust and compromising the longevity of concrete structures [15–17]. Fiber-reinforced bars, with their non-metallic composition, exhibit exceptional corrosion resistance [18]. Utilizing fiber composite bars in marine and water conservancy projects, in lieu of standard steel bars prone to corrosion and structural failure, can notably improve the endurance and efficiency of such concrete structures [19]. The diameter of fiber bars plays a crucial role in their concrete bonding performance [20,21]. Smaller diameter basalt fiber-reinforced polymer (BFRP) bars can reduce stress transmission length and minimize crack width. Furthermore, compared to conventional steel bars, fiber bars offer lower density and weight, thereby aiding in reducing structural loads when incorporated into concrete structures. Additionally, glass fiber-reinforced polymer (GFRP) and BFRP materials present a more economical choice than carbon fiber composites [22–24]. Despite the superior strength and stiffness of carbon fiber composites, their elevated cost limits their practical application in engineering. Conversely, GFRP and BFRP are cost-effective alternatives with favorable deformation characteristics. This comparative evaluation of fiber bar properties facilitates a better understanding of their suitability in diverse environments and offers more economical solutions for engineering applications.

Impact load is a frequent accidental load experienced during the service life of a structure. Its occurrence can result in severe damage to the structure or even lead to a rapid loss of bearing capacity. The mechanical properties of materials under dynamic loads exhibit distinct characteristics compared to those under static loading [25–27], known as the material's strain rate effect. In water conservancy projects, bridges, and other structures exposed to humid environments over prolonged periods, corrosion-resistant fiber-reinforced composite materials provide superior alternatives to traditional steel reinforcement materials.

Glass and basalt fiber bars stand out as common types of fiber composite reinforcements [28], warranting thorough exploration of their mechanical properties and failure mechanisms under dynamic loads due to the strain rate effect [29,30]. This study conducted a drop weight impact test on six fiber-reinforced concrete one-way plates to evaluate failure modes and diverse mechanical parameters, offering valuable insights for in-depth examinations of the mechanical characteristics of glass/basalt fiber-reinforced concrete plates when subjected to impact loads.

## 2. Experimental Program of Glass/Basalt Fiber-Reinforced Concrete One-Way Plate

### 2.1. Sampling Procedure

In this study, a total of 6 one-way plates were subjected to a drop weight impact test. The cement was made of Yueqing Conch brand 42.5 grade ordinary Portland cement, combined with river sand, gravel, and water. The specimen has geometric dimensions of 1200 mm in length, 400 mm in width, and 60 mm in height. Figure 1 illustrates the sizes of the fiber-reinforced concrete one-way plate and its internal reinforcement. The plate utilized glass/basalt fiber reinforcement, with longitudinal tension reinforcement at 6.5 mm diameter and 80 mm spacing, and transverse reinforcement at 6.5 mm diameter and 150 mm spacing. The concrete used in this study possesses a compressive strength of C30, and a 10 mm thick protective layer is employed. All fibers were tested after 28 days of curing. To facilitate transportation and testing, an 8 mm diameter lifting ring was installed on the upper surface of the specimen beam. The composition consisted of water, cement, sand, and gravel. The concrete mix proportions are detailed in Table 1.

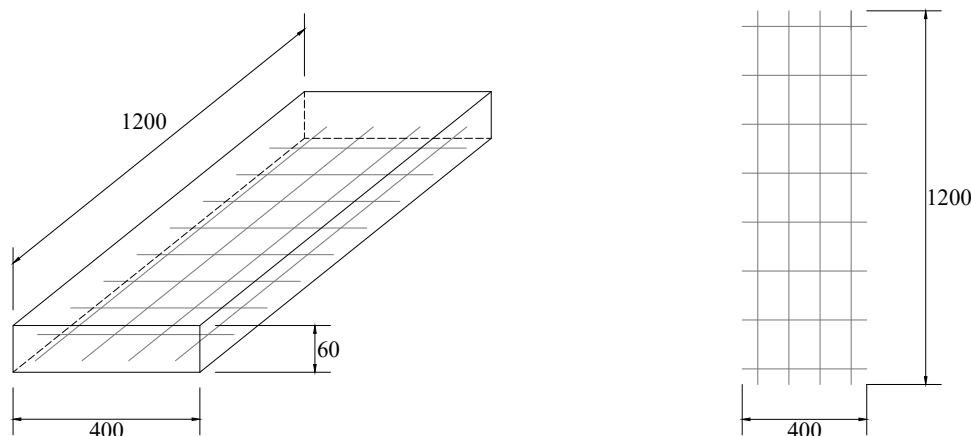


**Figure 1.** One-way plate dimensions and reinforcement diagram.

The specimens were categorized into two height groups, each consisting of three specimens, for impact testing. Glass and basalt fiber-reinforced specimens were subjected to impact testing at heights of 0.25 m, 0.5 m, and 1 m, aimed at assessing the performance of fiber-reinforced concrete under impact loads and elucidating the mechanical response of glass and basalt fiber reinforcements under varying conditions. This study investigated the failure mode and dynamic response characteristics of fiber-reinforced concrete one-way plates under falling weight impact loads, focusing on two key variables: the material of the tensile longitudinal bars and the height of the impact. Detailed parameters of the specimens can be found in Table 2.

**Table 1.** Glass/basalt fiber-reinforced concrete mass mix ratio.

Water–Cement Ratio	Water (kg)	Cement (kg)	Sand (kg)	Gravel (kg)
0.56	16.40	29.28	55.60	90.72

The objective of these experiments is to evaluate the performance of fiber-reinforced concrete when subjected to impact loads and to investigate the mechanical response of glass and basalt fiber reinforcements under different conditions. The study presents a comprehensive evaluation of the dynamic load behavior of fiber-reinforced concrete, providing valuable insights and credible references for the application of this material in engineering practices.

**Table 2.** Specimen parameters.

Specimen Number	Drop Weight (kg)	Drop Weight Height (m)	Specimen Age (d)	Design Impact Speed (m/s)
BLB-0.25m-1	100	0.25	28	2.21
BLB-0.5m-2	100	0.5	28	3.13
BLB-1.0m-3	100	1.0	28	4.43
XWB-0.25m-4	100	0.25	28	2.21
XWB-0.5m-5	100	0.5	28	3.13
XWB-1.0m-6	100	1.0	28	4.43

In test specimen BLB/XWB-A-B, BLB/XWB denotes the glass fiber-reinforced one-way plate and the basalt fiber-reinforced one-way plate tested under impact conditions. Here, A signifies the drop weight impact height, while B indicates the specific test plate number.

## 2.2. Impact Test Loading and Data Acquisition Devices

The impact test was conducted using a drop weight impact testing machine, comprising essential components such as rigid beams, guide rails, release mechanisms, drop

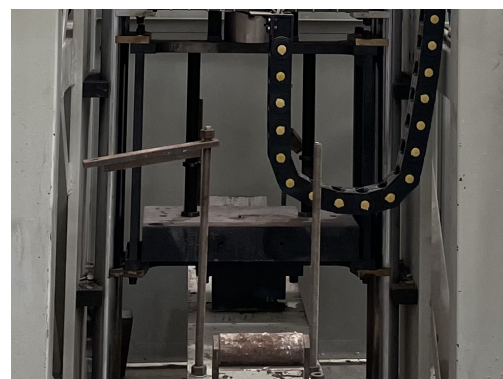
weights, hammer head control and lifting devices, as well as steel pedestals. The hammer head's maximum release height is 7.5 m, and its weight can be adjusted from 50 kg to 300 kg. This machine utilizes an electromagnet release system, activated by a button on the hammer head control and lifting device, as depicted in Figure 2. For the experiments detailed in this section, a 100 kg hammer head was used to apply a concentrated load at the mid-span of the beam body.



(a) Drop weight impact test loading device



(b) Hammer head control and lifting device



(c) Adjustable weighted drop weight

**Figure 2.** Drop weight impact test device.

The beam support is composed of a knife-edge support and a roller support. It adopts a two-section simply supported support. The detailed diagram of the support is shown in Figure 3. After the fiber-reinforced one-way plate is erected on the support, adjust the position of the plate so that the mid-span of the plate is parallel to the rigid base. Use a

pressure beam device composed of nuts and two rods to fix both ends of the plate on the support to prevent. During the impact of the falling weight, the specimen bounces off the support, causing test errors.

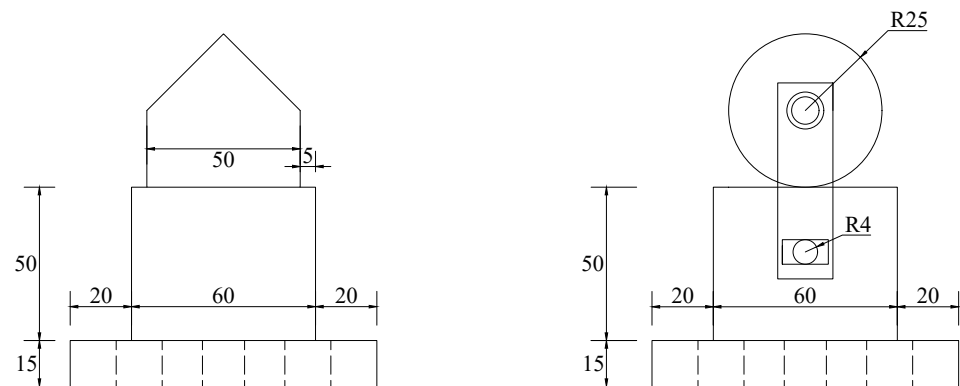


**Figure 3.** Bearing details.

The impact test data was gathered using the ultra-dynamic signal test analysis system DH-5960 manufactured by Jiangsu Donghua Testing Technology Co., Ltd., Jingjiang, China. This multi-channel system can simultaneously capture acceleration, displacement, strain, and other relevant data. The acquisition equipment setup is depicted in Figure 4, showcasing a sampling frequency of 100 kHz for this experiment. Specifically, four channels were dedicated to measuring plate and plate side strains, five channels for acceleration readings, and six channels for mid-span deflection of the specimen beam. Uniform sampling frequencies were applied across all channels.

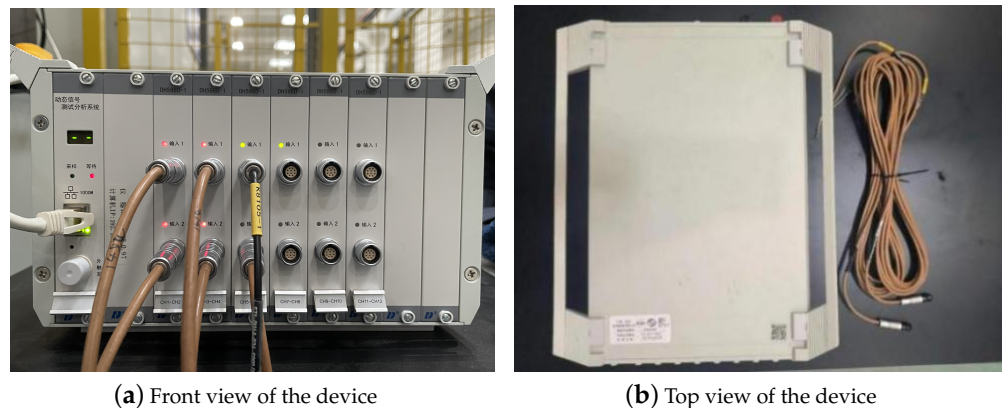


**Figure 4.** Hyperdynamic signal testing and analysis system.

Acceleration data is obtained through an IEPE piezoelectric acceleration sensor, model 1A532E, manufactured by Jiangsu Donghua Testing Technology Co., Ltd., capable of measuring within the range of  $\pm 10,000$  g. Positioned at the center of the hammer head, the sensor gasket is affixed using epoxy resin glue. Once the glue cures, the sensor can be properly oriented and secured. The installation of the acceleration sensor is depicted in Figure 5.

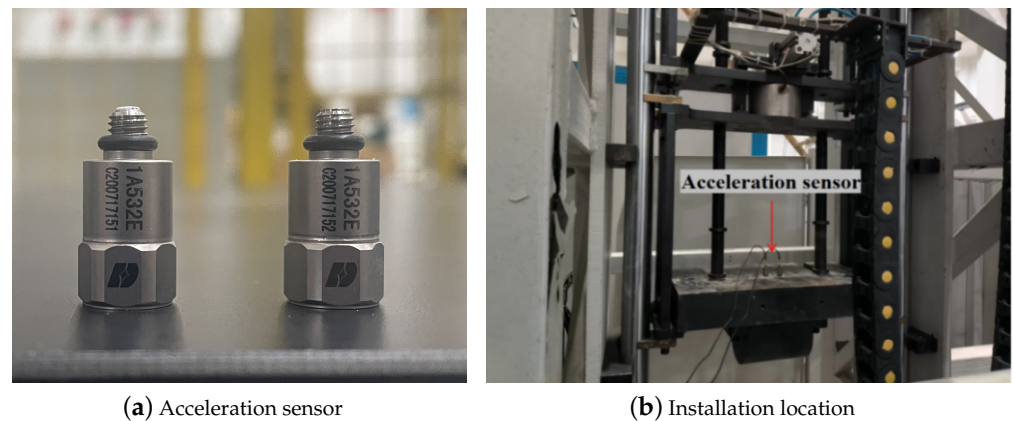


**Figure 5.** Acceleration sensor.

The mid-span deflection data of the test plate was captured using Panasonic's *HL – G125 – A – C5* standard laser displacement sensor. This sensor has a 250 mm measurement center distance and a  $\pm 150$  mm measurement range. During the drop weight impact test, the laser displacement sensor is positioned directly beneath the mid-span of the support steel plate, with the infrared laser directed at the specimen's mid-span through a designated opening. The sensor is securely attached to the support steel plate's underside using self-tapping screws. The laser projection display screen is mounted vertically at the steel plate's opening.

In order to accurately capture the development of cracks and damage in the test plate during impact testing, the *AE120M* high-speed camera from Hefei Fuhuang Junda High-Tech Information Technology Co., Ltd. was employed. The camera's specifications include a resolution of  $1280 \times 1024$  and an acquisition cycle of 1000 microseconds. It was connected to a computer for manual triggering via a data cable, and professional photography lighting was utilized to ensure proper illumination.

The primary data gathered in the drop weight impact test encompass the acceleration of the hammer head, the mid-span deflection of the test plate, and the concrete strain on both the plate and its side. Figure 6 illustrates the schematic layout of each sensor. Acceleration is monitored using acceleration sensors, while mid-span deflection is assessed through laser displacement sensors. The entire dataset is captured and processed by the ultra-dynamic signal testing and analysis system.

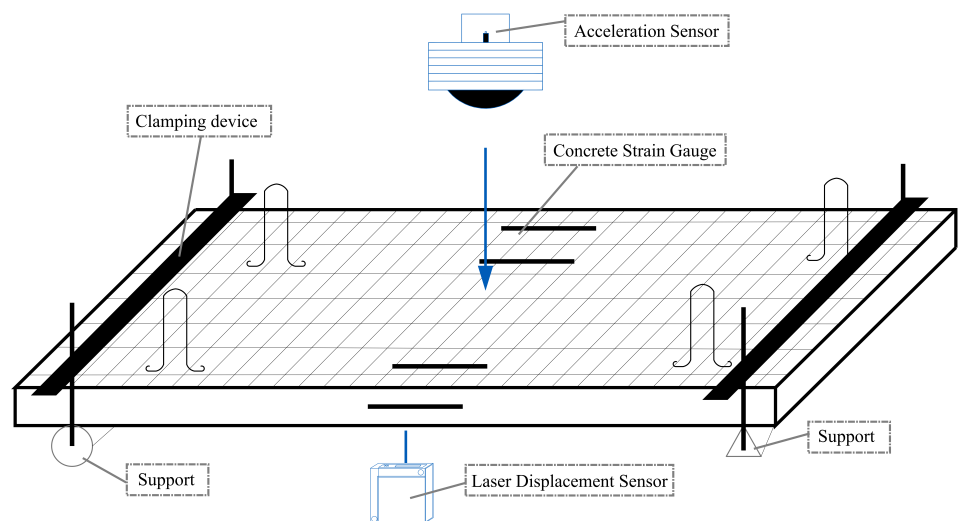


**Figure 6.** Sensor layout diagram.

### 2.3. Material Mechanical Properties

To investigate the material's mechanical properties thoroughly, this study conducted tests on the cubic compressive strength and axial compressive strength of concrete test blocks. Concrete beams were cast for each working condition, and three sides with a length of 150 mm were simultaneously prepared. The cube test blocks were cured for 28 days following the standard procedure. Testing was performed using an electronic universal pressure testing machine from Jinan Tianchen Testing Machine Manufacturing Co., Ltd. (Jinan, China), with consideration given to ensuring test accuracy by averaging the results, as depicted in Figure 7. Three test blocks of each age were tested and the average value was taken and 0.76 times the concrete cube compressive strength value was taken as the concrete axial compressive strength. The test results are shown in Table 3.

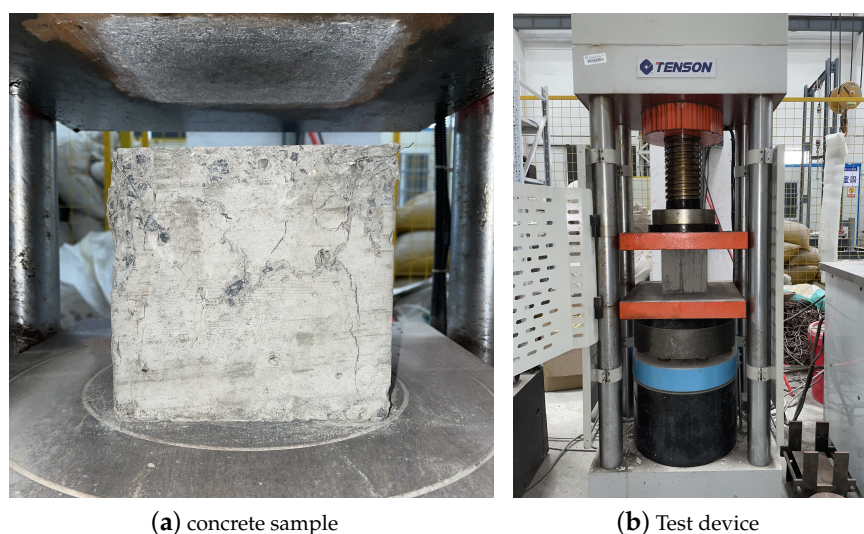


Figure 7. Concrete compressive strength test.

Table 3. Concrete compressive strength test results.

Test Block Number	Compressive Strength (MPa)	Concrete Axial Compressive Strength (MPa)
Test block 1	33.7	25.6
Test block 2	31.8	25.6
Test block 3	35.5	25.6

Glass fiber rebar and basalt fiber rebar are fabricated using glass fiber or basalt fiber as reinforced material, coupled with high-performance resin and high-strength fiber through a pultrusion process. In comparison to traditional steel rebar, they exhibit superior tensile properties, are lightweight, high-strength, corrosion-resistant [21,31], easy to cut, and non-magnetic. The tensile tests were conducted using the WAW – 600D microcomputer-controlled electro-hydraulic servo hydraulic universal testing machine from Jinan Chenda Testing Machine Manufacturing Co., Ltd. (Jinan, China), resulting in measured tensile strengths of 896 MPa for glass fiber bars and 883 MPa for basalt fiber bars. The tensile test of the fiber-reinforced material is depicted in Figure 8, with the mechanical property test outcomes detailed in Table 4.

Table 4. Mechanical properties of fiber-reinforced materials.

Fiber Tendon Category	Nominal Diameter (mm)	Tensile Strength (MPa)	Elastic Modulus (GPa)	Unit Weight (g/m)	Shear Strength (MPa)
Glass fiber bars	6.5	896	46	77.4	150
Basalt fiber bars	6.5	883	45	78.5	150

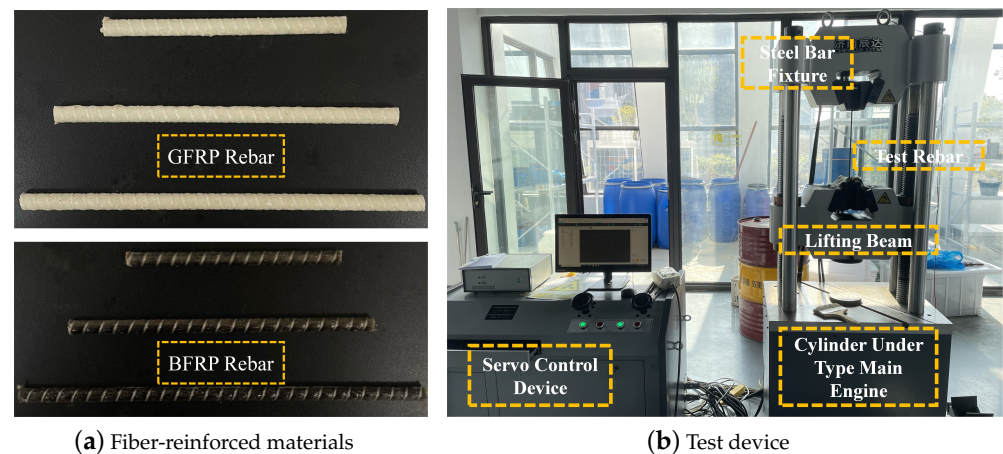


**Figure 8.** Tensile test of fiber-reinforced materials.

### 3. Results and Discussion

#### 3.1. Analysis of the Morphology of Test Plate Failure

Under the impact load, concrete structures are subjected to damage. The yielding of steel bars in the tension zone becomes crucial to monitor, as evident deformations, cracks, and fractures may occur. Compression areas typically experience significant crushing damage. Additionally, detailed description of crack propagation is necessary. Impact loading can lead to the formation of cracks of various types and sizes on the test sample's surface, potentially expanding within the concrete and compromising the overall stability and load-bearing capacity.

The experimental findings in this paper delineate the damage characteristics of the test specimens. During the impact test, all six fiber-reinforced concrete one-way plates exhibited bending damage, with failure patterns detailed in Figures 9 and 10. When utilizing the same type of fiber reinforcement, the degree of damage to the one-way plates gradually increased as the height of the falling weight escalated. Notably, at drop heights of 0.25 m and 0.5 m, the glass/basalt fiber bar specimens exhibited slight damage, with relatively narrow cracks along the mid-span and sides of the plates and only a few perpendicular tiny cracks on the surface at the mid-span impact zone. However, at a drop height of 1 m, the damage level significantly intensified, manifesting in pronounced bending of the plates, concrete breakage, cracks, and fracture of fiber bars in the tension zone at the plate bottom.

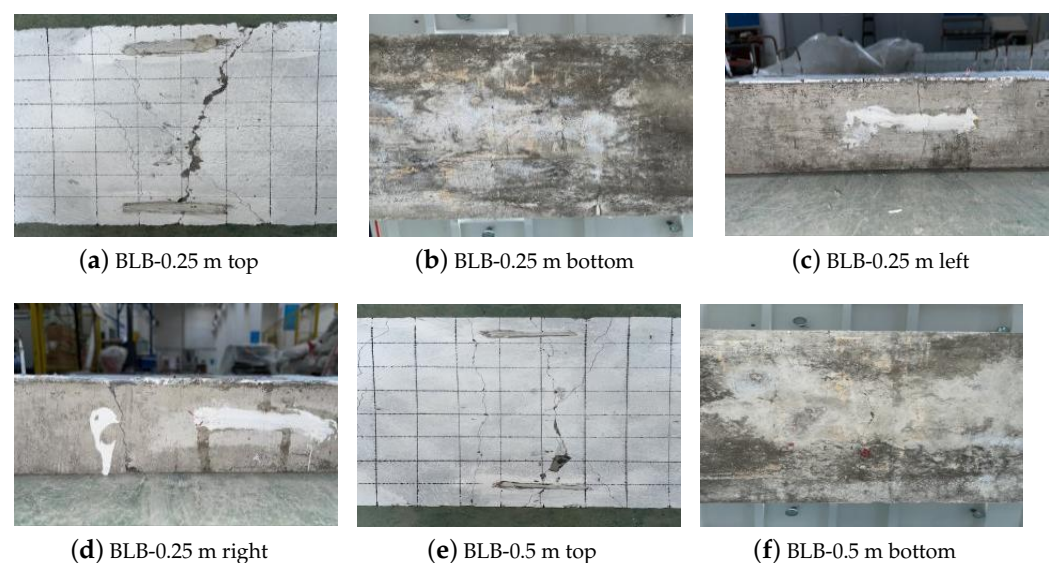


**Figure 9.** Cont.

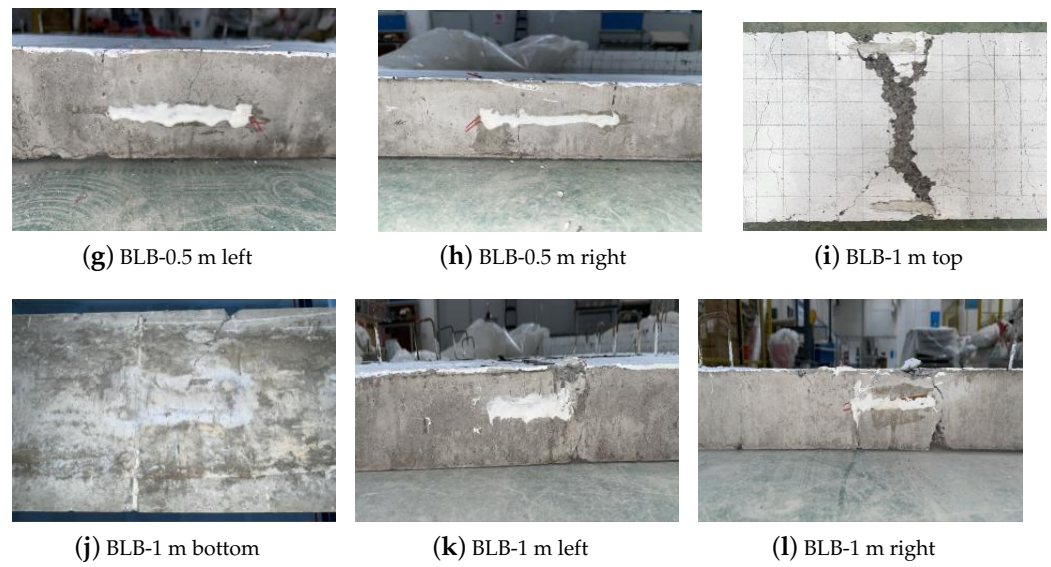


**Figure 9.** Failure pattern of glass fiber-reinforced concrete one-way plate.

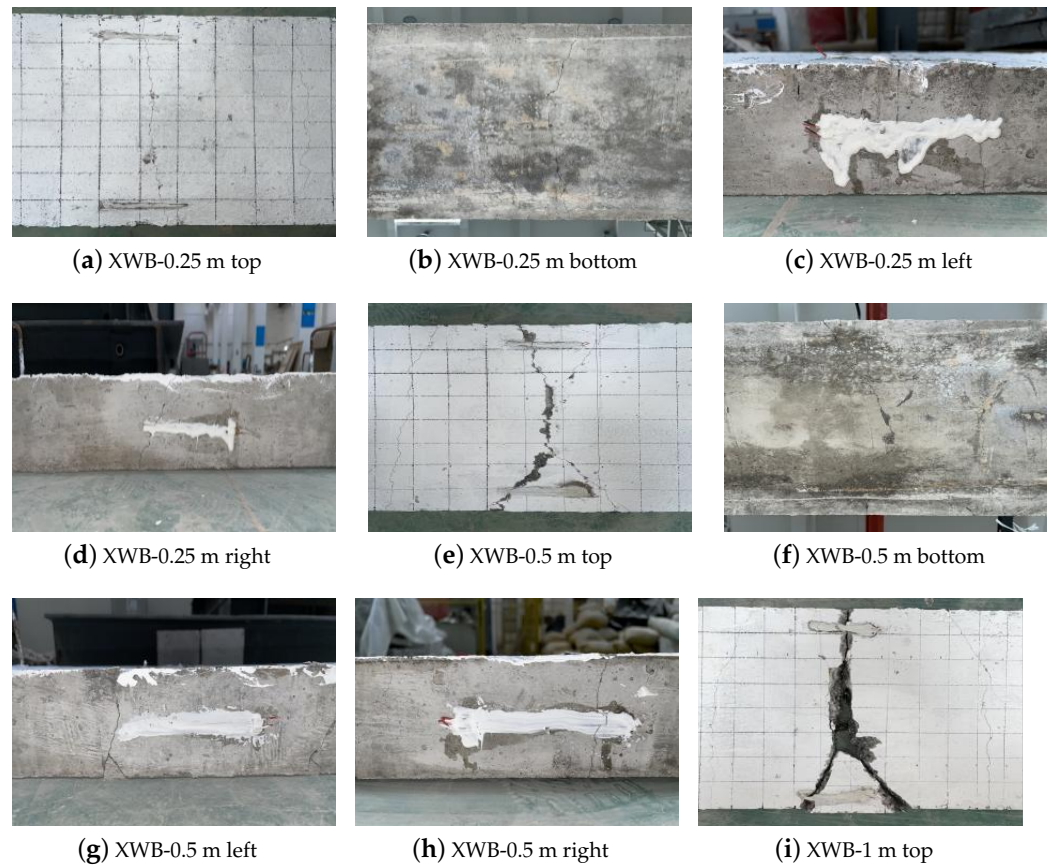


**Figure 10.** Cont.

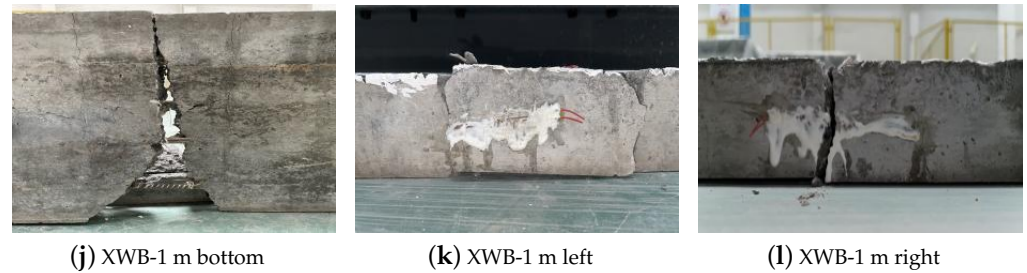


**Figure 10.** Failure pattern of basalt fiber-reinforced concrete one-way plate.

Distinct failure modes emerged for glass and basalt fiber-reinforced plates under identical impact conditions. When subjected to a 1 m falling weight, the glass fiber-reinforced plate displayed cracks parallel to the long-side reinforcement, forming intricate networks of multiple fine cracks. In contrast, the basalt fiber-reinforced plate exhibited less prominent and fewer edge reinforcement direction cracks, yet wider perpendicular through cracks on the plate surface.

The inherent characteristics of fiber bars, including poor shear resistance, limited elastic modulus, and absence of a clear yield point, contribute to the one-way plate's brittle failure behavior under impact loading. To comprehensively document the impact process, a high-speed camera was employed to capture key test phases, as depicted in Figures 11 and 12.

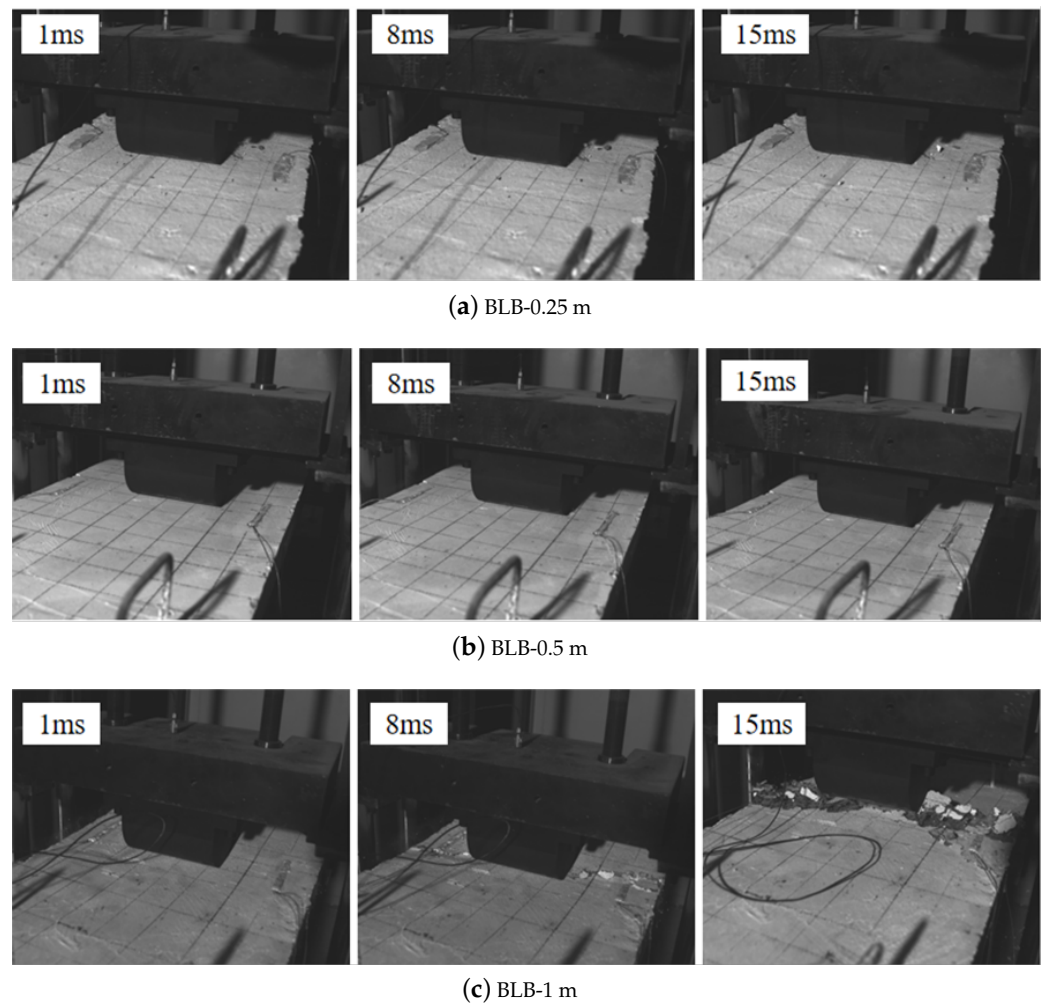


**Figure 11.** Failure process of glass fiber-reinforced concrete one-way plate.

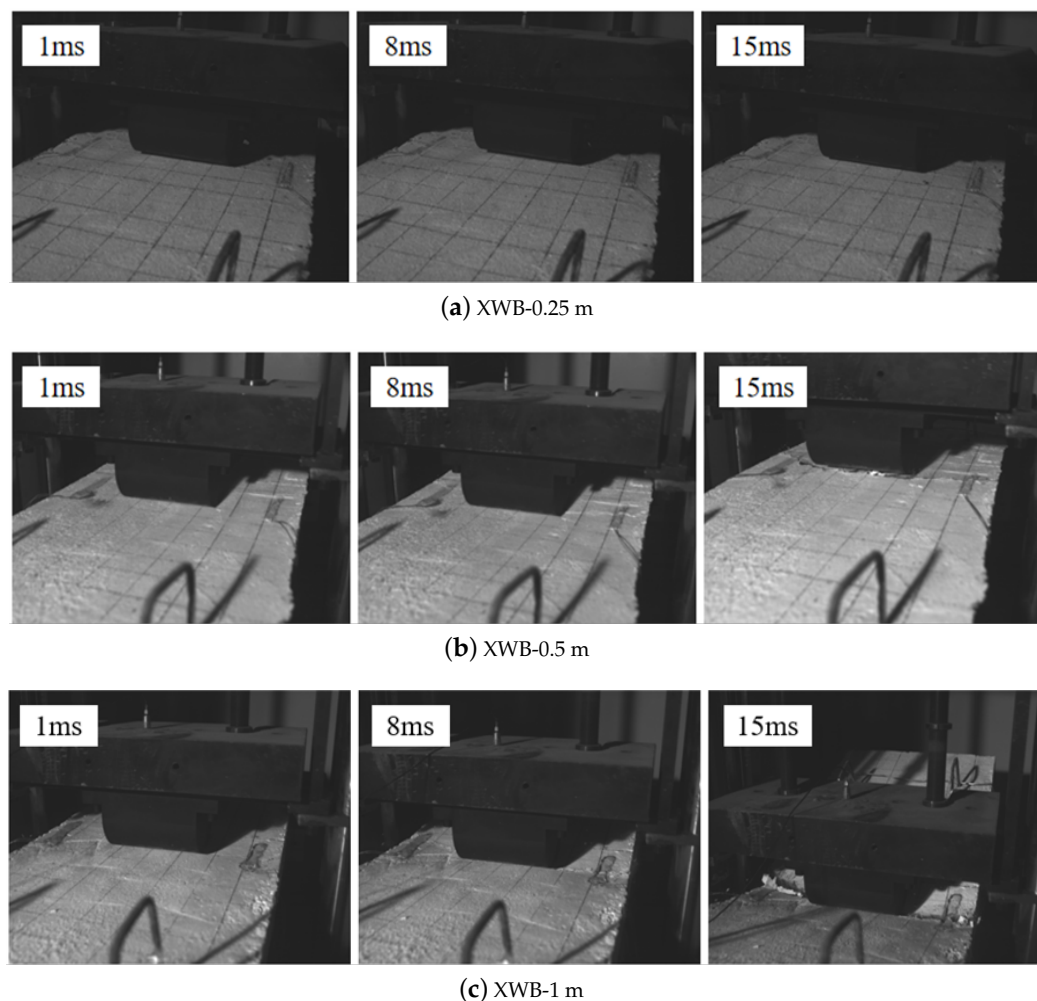


**Figure 12.** Failure process of basalt fiber-reinforced concrete one-way plate.

### 3.2. Analysis of Impact Force and Mid-Span Deflection Time History Curves

This study investigates how two variables, namely the longitudinal tension steel material and drop weight impact height, influence the impact performance of concrete one-way plates. The dynamic response and mechanical characteristics of the test plates are evaluated by analyzing the time history curves of impact force and mid-span deflection. The impact force and mid-span deflection time history curves for each specimen are illustrated in Figure 13. Following impact by the falling weight on the top surface of the test plate, the impact force time history curves of the one-way plates under varied loading conditions exhibit similar patterns in the 30 ms time history curve. These curves typically feature a high-amplitude waveform followed by several low-amplitude waveforms, resembling findings from previous studies. Initially, each specimen experiences a rapid increase to a peak impact force, followed by a swift decrease, forming the primary waveform. With continued impact from the falling weight, the waveform stabilizes gradually. Higher impact speeds result in shorter waveform durations and increased peak impact force values under consistent impact quality. Following the initial impact, when the hammer head contacts the plate, the first peak in the impact force time history curve is recorded, triggering downward displacement of the plate and subsequent mid-span deflection growth. Subsequent impacts observe reduced heights due to the effective vibration damping properties of the composite fiber bars.

The initial significant impact was crucial in capturing the impact force time history curve and mid-span deflection time history curve. To mitigate instrument noise and micro-current interference, the impact force and mid-span deflection curves were filtered,

correcting any invalid distortion or instrument error values. Processed impact force and mid-span deflection time history curves are presented in Figure 13.

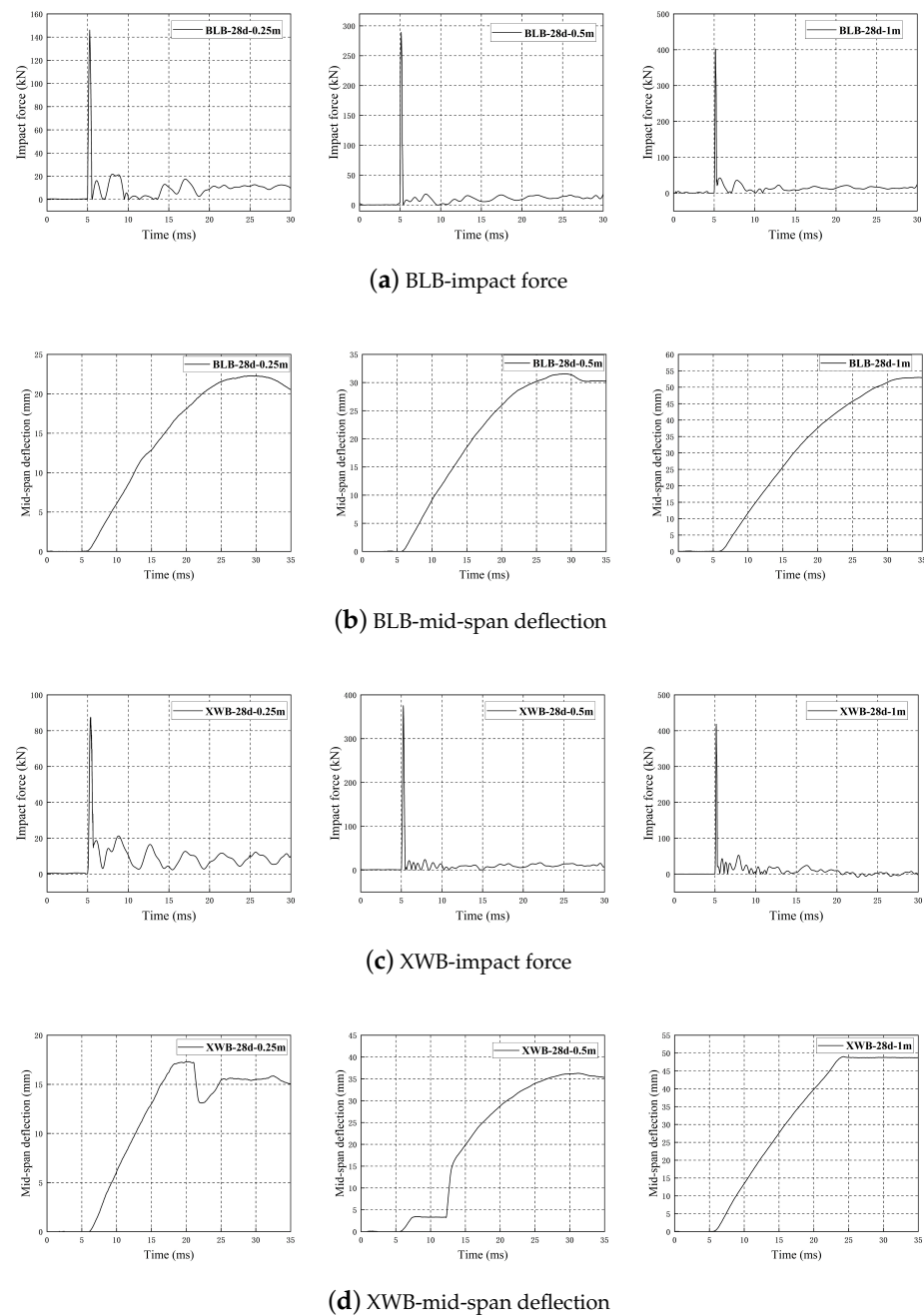


**Figure 13.** Impact force and mid-span deflection time history curves.

The impact test results of glass/basalt fiber-reinforced concrete one-way plates at various drop heights are detailed in Table 5. The analysis of the mid-span deflection time history curve and impact test outcomes reveals a direct relationship between the increase in drop weight impact height and the corresponding rise in mid-span deflection—a positive correlation exists between these variables. In general, glass fiber-reinforced concrete one-way plates exhibit superior impact deformation capabilities compared to basalt fiber-reinforced counterparts, as indicated by slightly greater mid-span deflection values. Moreover, the peak impact force demonstrates a positive correlation with the speed of the falling weight; an escalation in impact speed leads to a proportional increase in peak impact force. Notably, between drop heights of 0.25 m and 0.5 m, a distinct rebound

process is observable. However, at a height of 1 m, the fiber-reinforced concrete one-way plate undergoes concrete cracking in the compression zone and longitudinal reinforcement rupture in the tension zone, halting any rebound.

For instance, at a drop height of 0.25 m, the calculated impact speed is m/s. Data analysis reveals more prominent deformation in glass fiber-reinforced concrete one-way plates. Notably, the mid-span deflection time history curve illustrates a clear rebound process at a 0.25 m height, with a residual displacement at the mid-span ranging from 15 to 20 mm.

**Table 5.** Glass/basalt fiber-reinforced concrete mass mix ratio.

Specimen Number	Weight of Falling Weight (kg)	Height of Falling Weight (m)	Failure Pattern	Impact Speed (m/s)	Mid-Span Deflection (mm)	Impact Force (kN)
BLB-0.25m-①	100	0.25	Bending damage	2.21	22.991	142.07
BLB-0.5m-②	100	0.5	Bending damage	3.13	36.276	289.21
BLB-1.0m-③	100	1.0	Bending damage	4.43	52.991	402.16
XWB-0.25m-④	100	0.25	Bending damage	2.21	17.272	87.57
XWB-0.5m-⑤	100	0.5	Bending damage	3.13	31.551	375.44
XWB-1.0m-⑥	100	1.0	Bending damage	4.43	48.997	418.24

With the falling weight's height increasing to 0.5 m, the theoretical impact velocity jumps to 3.13 m/s. Comparative analysis shows that in this scenario, peak impact force and mid-span deflection values are higher than those at a 0.25 m drop height, with a faster rate of reaching these peak values. The springback of the specimen within a 35 ms interval is approximately 3 mm, contributing to an increased mid-span residual displacement.

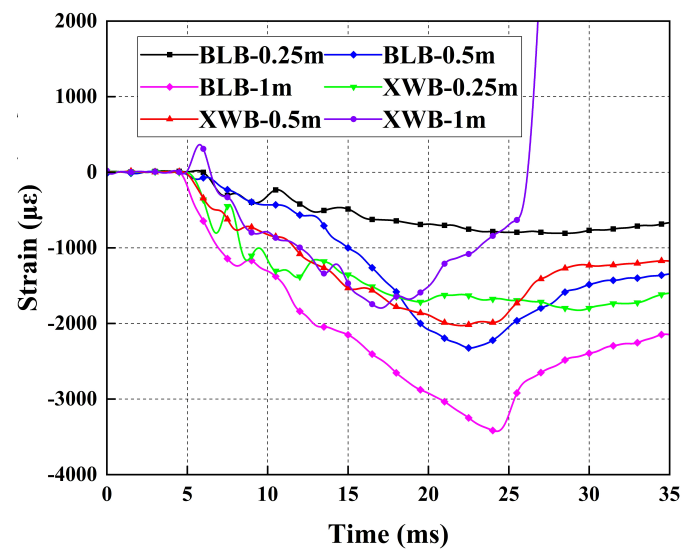
At a 1 m drop height, the theoretical impact velocity climbs to 4.43 m/s. The tests indicate slightly larger mid-span deflection in glass fiber-reinforced concrete plates compared to basalt fiber-reinforced counterparts. Notably, the specimen exhibited minimal rebound due to concrete cracking at the mid-span and tensile fiber bar fracture. The impact force time history curve illustrates a quicker approach to peak force values, which are closely matched between the two fiber-reinforced concrete specimens. Moreover, increased drop weight height leads to heightened mid-span deflection and residual displacement, with glass fiber-reinforced concrete plates showcasing greater deformation and intricate crack patterns. This behavior suggests reduced overall deformation resistance under higher impact loads.

### 3.3. Analysis of Plate and Plate Side Strain Time History Curves

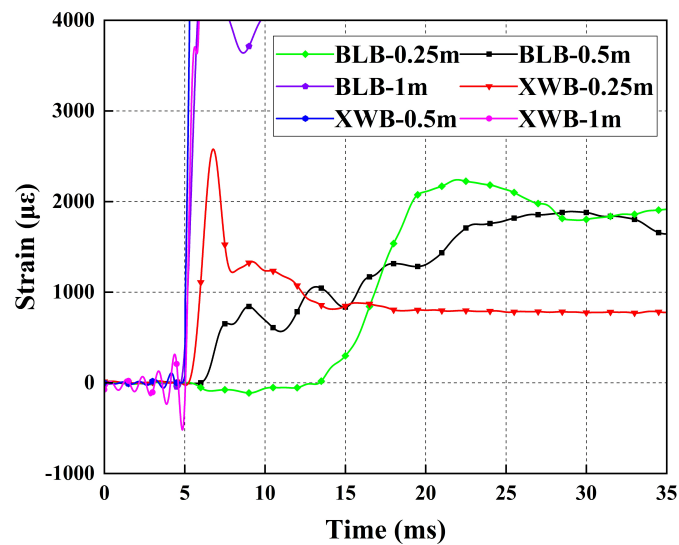
The strain rate significantly impacts concrete failure, particularly at high rates where the internal microstructure fails to adjust adequately to changing loading conditions, leading to a more brittle failure mode. The strain-time history curves of glass fiber-reinforced and basalt fiber-reinforced concrete one-way plates from this study are presented in Figure 14. Steel bar strain is negative during compression and positive during tension. The change in the strain curve begins to show changes at a time point of about 5 ms.

As depicted in Figure 14a, all hybrid strain gauges on each one-way plate experience compression under impact loads, with strain values rising as the drop weight height increases. For drop heights of 0.25 m and 0.5 m, the strain in the one-way plate during low-speed impacts is generally lower. The increased height and speed of the falling weight under impact loading cause a corresponding rise in the concrete strain rate. The experimental findings corroborate this trend. Evaluation of strain values across different fiber-reinforced concrete one-way plates reveals higher strain levels in glass fiber-reinforced plates compared to basalt fiber-reinforced ones, indicating superior impact performance of glass fiber bars over basalt fiber bars.

Figure 14b demonstrates a rapid rise in plate side strain of the fiber-reinforced one-way plate after 5 ms, followed by a decrease and stabilization. Despite some variations, the overall curve trends are similar. The one-way plate exhibits brittle failure under impact, with strain gauges on the side failing concurrently with concrete matrix cracking. Effective strain values within the initial 35 ms of contact with the drop hammer indicate positive values, signifying tension on the plate side. Increasing the drop height results in higher peak impact force and side plate strain values.



(a) Plate strain time history curve



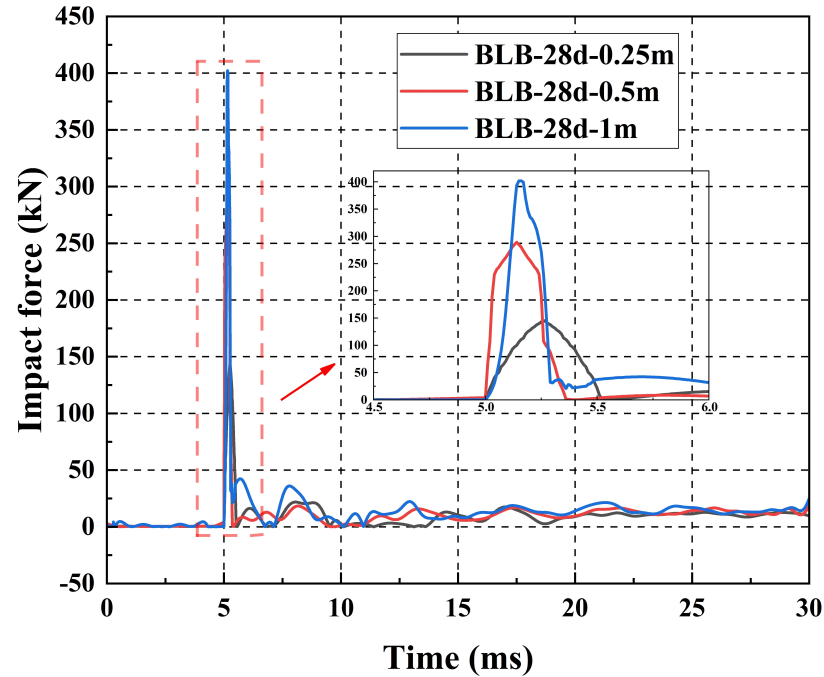
(b) Plate side strain time history curve

Figure 14. Strain time history curve.

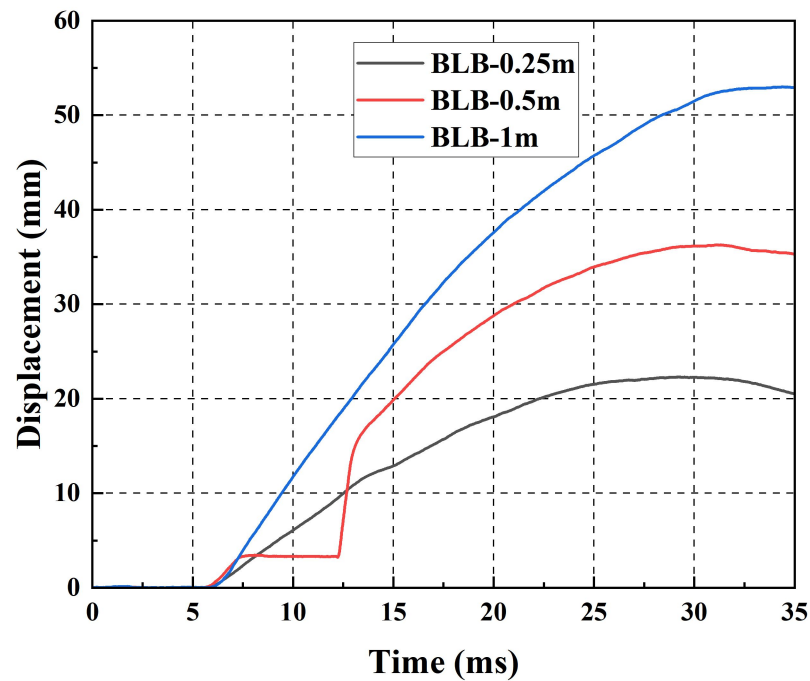
The fiber-reinforced concrete one-way plate effectively considers the strain rate effect on material properties, mitigating its adverse impact to a certain degree. Integration of fiber bars with the concrete diminishes the impact load, enhancing structural impact resistance and safety. The analysis of strain time history curves yields valuable insights into the deformation and stress patterns of fiber-reinforced concrete one-way plates under diverse impact loads.

### 3.4. Analysis of Different Fiber Reinforcement Materials on the Dynamic Response

Figure 15 illustrates the impact force time history curve and mid-span deflection time history curve of six one-way fiber-reinforced concrete plates fabricated with distinct fiber materials.

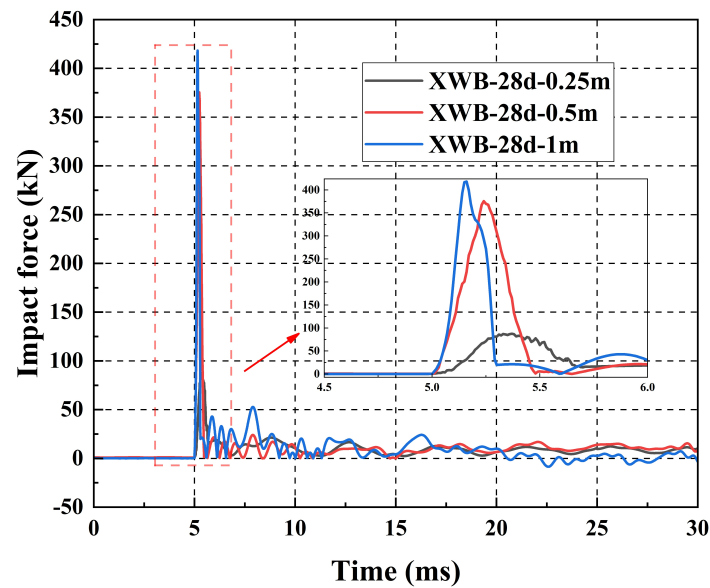


(a)

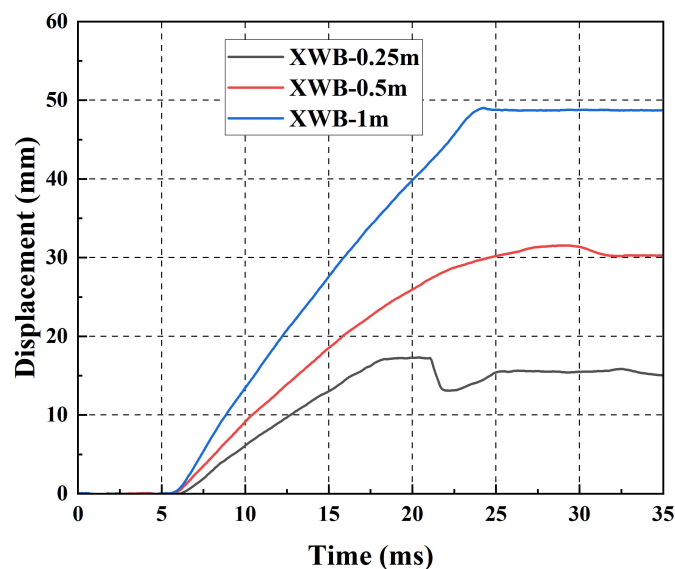


(b)

Figure 15. *Cont.*



(c)



(d)

**Figure 15.** Comparison of impact force and mid-span deflection time history of different fiber reinforcement materials. (a) Impact force time history curve for glass fiber reinforcement material, (b) Mid-span deflection time history curve for glass fiber reinforcement material, (c) Impact force time history curve for basalt fiber reinforcement material, (d) Mid-span deflection time history curve for basalt fiber reinforcement material.

It is evident from the graph that as the impact height on the two types of fiber-reinforced concrete plates increases, there is a linear escalation in peak impact force and the peak deflection at mid-span also increases accordingly. Comparing the results, it is noteworthy that across three drop weight impact heights, the glass fiber-reinforced concrete one-way slab exhibits slightly higher mid-span deflection peaks than its basalt fiber-reinforced counterpart. Glass fiber-reinforced concrete displays enhanced resilience to impact deformation and superior impact toughness. This superiority can be attributed to two primary factors: firstly, the superior deformation capabilities of glass fibers compared to basalt fibers; secondly, the special manufacturing process involving blending highly elastic fiber materials with resin and shaping them into composite materials, resulting in

excellent vibration damping properties and a high natural vibration frequency. Furthermore, glass fiber bars exhibit stronger adhesion compared to basalt fiber bars, enhancing their interaction with the concrete matrix's coarse and fine aggregates and contributing to an overall performance enhancement.

#### 4. Conclusions

This study conducted a drop weight impact test on six fiber-reinforced concrete one-way plates, analyzed the damage patterns and various mechanical indicators of the plates, and investigated the mechanical properties of glass/basalt fiber-reinforced concrete plates under impact loads. The conclusions derived from the study are as follows:

(1) As the loading rate increases, the degree of damage in fiber-reinforced concrete one-way plates demonstrates an upward trend. The peak deflection value and residual displacement at the mid-span of the specimen also increase, signifying the gradual emergence of the impact load's influence on the plate. Notably, glass fiber-reinforced concrete specimens exhibit more pronounced deformation and intricate crack formations during the impact process, indicating a higher sensitivity to impact loads.

(2) Glass/basalt fiber-reinforced composites display favorable vibration damping properties, characterized by significant residual displacement, minimal rebound, and rapid decay post-vibration excitation. These characteristics highlight the composite material's notable damping effect, which effectively retards vibration propagation under impact loads, thus enhancing the stability and safety of structures.

(3) During the impact of the falling weight, the fiber-reinforced one-way plate experiences compression, while the concrete on the plate's side undergoes tension. In general, glass fiber-reinforced one-way plates demonstrate slight advantages in impact resistance compared to basalt fiber-reinforced counterparts. This suggests that glass fiber bars are better equipped to preserve structural integrity and stability when subjected to impact loads, possibly due to their higher strength and superior deformation capabilities.

(4) The peak impact force and mid-span deflection of glass fiber-reinforced/basalt fiber-reinforced concrete one-way slabs exhibit a positive correlation with the height of the falling weight during impact loading. Increasing the falling weight height results in higher peak impact force and mid-span deflection values.

(5) Across identical falling weight masses and impact heights, all fiber-reinforced concrete one-way panels experience flexural damage. Glass fiber-reinforced panels demonstrate superior impact deformation resilience compared to basalt fiber-reinforced ones.

In conclusion, this study underscores the significant influence of loading rate and fiber bar type on the mechanical properties of fiber-reinforced concrete one-way plates, providing valuable insights for the assessment and design of such materials in practical engineering applications.

**Author Contributions:** L.L., J.C., S.L. and H.C. mostly contributed to the design of the manuscript. L.L. and H.C. carried out data collection and processing. L.L., X.H., S.L. and H.C. participated in the sample preparation and experimental steps. J.C. and S.L. write and revise the paper. All authors have read and agreed to the published version of the manuscript.

**Funding:** The authors are appreciated for the financial support provided by the Natural Science Foundation of Zhejiang Province (No. LY21E080002), the Science Foundation of the Wenzhou University of Technology (No. ky202202), the Innovation Project on Technology Services funded by the Wenzhou Science and Technology Association (Project No. NLTS0039), and the National Natural Science Foundation of China (51608393).

**Data Availability Statement:** The data that support the findings of this study are available from the corresponding author upon reasonable request.

**Acknowledgments:** The authors would like to thank all the anonymous referees for their constructive comments and suggestions.

**Conflicts of Interest:** Author Xin Huang was employed by the company Wenzhou Traffic Engineering Testing and Testing Co., Ltd. The remaining authors declare that the research was conducted in the absence of any commercial or financial relationships that could be construed as a potential conflict of interest.

## References

1. Mohamed, O.A.; Al Hawat, W.; Keshawarz, M. Durability and mechanical properties of concrete reinforced with basalt fiber-reinforced polymer (BFRP) bars: Towards sustainable infrastructure. *Polymers* **2021**, *13*, 1402. [[CrossRef](#)]
2. Yang, K.; Wu, Z.; Zheng, K.; Shi, J. Shear behavior of regular oriented steel fiber-reinforced concrete beams reinforced with glass fiber polymer (GFRP) bars. *Structures* **2024**, *63*, 106339. [[CrossRef](#)]
3. Rosa, I.C.; Firmo, J.P.; Correia, J.R.; Mazzuca, P. Influence of elevated temperatures on the bond behaviour of ribbed GFRP bars in concrete. *Cem. Concr. Compos.* **2021**, *122*, 104119. [[CrossRef](#)]
4. Abedini, M.; Mutalib, A.A. Investigation into damage criterion and failure modes of RC structures when subjected to extreme dynamic loads. *Arch. Comput. Methods Eng.* **2020**, *27*, 501–515. [[CrossRef](#)]
5. Anas, S.M.; Alam, M.; Umair, M. Experimental and numerical investigations on performance of reinforced concrete slabs under explosive-induced air-blast loading: A state-of-the-art review. *Structures* **2021**, *31*, 428–461. [[CrossRef](#)]
6. Xu, J.; Wu, C.; Li, Z.X. Analysis of direct shear failure mode for RC slabs under external explosive loading. *Int. J. Impact Eng.* **2014**, *69*, 136–148. [[CrossRef](#)]
7. Van den Einde, L.; Zhao, L.; Seible, F. Use of FRP composites in civil structural applications. *Constr. Build. Mater.* **2003**, *17*, 389–403. [[CrossRef](#)]
8. Yin, S.P.; Hua, Y.T.; Xu, S.L. A review on research progress and application of concrete structures internally reinforced with FRP bars. *J. Build. Struct.* **2021**, *42*, 134.
9. Elgabbas, F.; Ahmed, E.A.; Benmokrane, B. Physical and mechanical characteristics of new basalt-FRP bars for reinforcing concrete structures. *Constr. Build. Mater.* **2015**, *95*, 623–625. [[CrossRef](#)]
10. Protchenko, K.; Zayoud, F.; Urbański, M.; Szmigiera, E. Tensile and shear testing of basalt fiber reinforced polymer (BFRP) and hybrid basalt/carbon fiber reinforced polymer (HFRP) bars. *Materials* **2020**, *13*, 5839. [[CrossRef](#)] [[PubMed](#)]
11. He, J.; Lei, D.; She, Z.; Xi, B. Investigation on bonding behavior of basalt fiber reinforced polymer (BFRP) sheet reinforced concrete beam. *J. Build. Eng.* **2023**, *75*, 106963. [[CrossRef](#)]
12. Zou, R.; Liu, F.; Xiong, Z.; He, S.; Li, L.; Wei, W. Experimental study on fatigue bond behaviour between basalt fibre-reinforced polymer bars and recycled aggregate concrete. *Constr. Build. Mater.* **2021**, *270*, 121399. [[CrossRef](#)]
13. Hajiloo, H.; Green, M.F.; Gales, J. Mechanical properties of GFRP reinforcing bars at high temperatures. *Constr. Build. Mater.* **2018**, *162*, 142–154. [[CrossRef](#)]
14. Rosa, I.C.; Firmo, J.P.; Correia, J.R. Experimental study of the tensile behaviour of GFRP reinforcing bars at elevated temperatures. *Constr. Build. Mater.* **2022**, *324*, 126676. [[CrossRef](#)]
15. Qu, F.; Li, W.; Dong, W.; Tam, V.W.; Yu, T. Durability deterioration of concrete under marine environment from material to structure: A critical review. *J. Build. Eng.* **2021**, *35*, 102074. [[CrossRef](#)]
16. James, A.; Bazarchi, E.; Chiniforush, A.A.; Aghdam, P.P.; Hosseini, M.R.; Akbarnezhad, A.; Martek, I.; Ghodoosi, F. Rebar corrosion detection, protection, and rehabilitation of reinforced concrete structures in coastal environments: A review. *Constr. Build. Mater.* **2019**, *224*, 1026–1039. [[CrossRef](#)]
17. Chen, J.; Agostini, F.; Shen, W.; Shao, J.; Bourbon, X.; Liu, S. Experimental and numerical studies of a reinforced concrete component subjected to corrosion. *Mech. Res. Commun.* **2023**, *129*, 104076. [[CrossRef](#)]
18. Ahmed, A.; Guo, S.; Zhang, Z.; Shi, C.; Zhu, D. A review on durability of fiber reinforced polymer (FRP) bars reinforced seawater sea sand concrete. *Constr. Build. Mater.* **2020**, *256*, 119484. [[CrossRef](#)]
19. Naser, M.Z.; Hawileh, R.A.; Abdalla, J.A. Fiber-reinforced polymer composites in strengthening reinforced concrete structures: A critical review. *Eng. Struct.* **2019**, *198*, 109542. [[CrossRef](#)]
20. Mohebi, Z.H.; Bahnamiri, A.B.; Dehestani, M. Effect of polypropylene fibers on bond performance of reinforcing bars in high strength concrete. *Constr. Build. Mater.* **2019**, *215*, 401–409. [[CrossRef](#)]
21. Xiao, J.; Zeng, H.; Huang, H.; Liu, L.; Li, L.; Yuan, B.; Zhong, Z. Experimental Investigation on the Influence of Strength Grade on the Surface Fractal Dimension of Concrete under Sulfuric Acid Attack. *Buildings* **2024**, *14*, 713. [[CrossRef](#)]
22. Tao, Y.; Hadigheh, S.A.; Wei, Y. Recycling of glass fibre reinforced polymer (GFRP) composite wastes in concrete: A critical review and cost benefit analysis. *Structures* **2023**, *53*, 1540–1556. [[CrossRef](#)]
23. Li, C.; Xian, G.; Li, H. Effect of postcuring immersed in water under hydraulic pressure on fatigue performance of large-diameter pultruded carbon/glass hybrid rod. *Fatigue Fract. Eng. Mater. Struct.* **2019**, *42*, 1148–1160. [[CrossRef](#)]
24. Lal, H.M.; Uthaman, A.; Li, C.; Xian, G.; Thomas, S. Combined effects of cyclic/sustained bending loading and water immersion on the interface shear strength of carbon/glass fiber reinforced polymer hybrid rods for bridge cable. *Constr. Build. Mater.* **2022**, *314*, 125587. [[CrossRef](#)]
25. Zhang, Q.B.; Zhao, J. Determination of mechanical properties and full-field strain measurements of rock material under dynamic loads. *Int. J. Rock Mech. Min. Sci.* **2013**, *60*, 423–439. [[CrossRef](#)]

26. Li, L.; Wang, H.; Wu, J.; Du, X.; Zhang, X.; Yao, Y. Experimental and numerical investigation on impact dynamic performance of steel fiber reinforced concrete beams at elevated temperatures. *J. Build. Eng.* **2022**, *47*, 103841. [[CrossRef](#)]
27. Lee, J.Y.; Yuan, T.; Shin, H.O.; Yoon, Y.S. Strategic use of steel fibers and stirrups on enhancing impact resistance of ultra-high-performance fiber-reinforced concrete beams. *Cem. Concr. Compos.* **2020**, *107*, 103499. [[CrossRef](#)]
28. Conforti, A.; Zerbino, R.; Plizzari, G.A. Influence of steel, glass and polymer fibers on the cracking behavior of reinforced concrete beams under flexure. *Struct. Concr.* **2019**, *20*, 133–143. [[CrossRef](#)]
29. Qin, W.; Hui, Z.; Zhang, P.; Zhang, Z.; Li, M.; Xie, P. Experimental study on shearing capacity of concrete beams longitudinal reinforced with steel fiber composite bars and BFRP bars. *J. Build. Struct.* **2022**, *43*, 209.
30. Elgabbas, F.; Vincent, P.; Ahmed, E.A.; Benmokrane, B. Experimental testing of basalt fiber-reinforced polymer bars in concrete beams. *Compos. Part Eng.* **2016**, *91*, 205–218. [[CrossRef](#)]
31. Xiao, J.; Huang, L.; He, Z.; Qu, W.; Li, L.; Jiang, H.; Zhong, Z.; Long, X. Probabilistic models applied to concrete corrosion depth prediction under sulfuric acid environment. *Measurement.* **2024**, 114807. [[CrossRef](#)]

**Disclaimer/Publisher's Note:** The statements, opinions and data contained in all publications are solely those of the individual author(s) and contributor(s) and not of MDPI and/or the editor(s). MDPI and/or the editor(s) disclaim responsibility for any injury to people or property resulting from any ideas, methods, instructions or products referred to in the content.